The structures of cationic gold clusters probed by far-infrared spectroscopy

Received 00th January 20xx,
Accepted 00th January 20xx

DOI: 10.1039/x0xx00000x

Piero Ferrari[a,*], Gao-Lei Hou[a], Olga V. Lushchikova[b], Florent Calvo[c], Joost M. Bakker[b], Ewald Janssens[a,*]

Determining the precise structure of small gold clusters is an essential step towards understanding their chemical and physical properties. Due to the relativistic nature of gold, its clusters remain planar (2D) up to appreciable sizes. Ion mobility experiments have suggested that positively charged gold clusters adopt three-dimensional (3D) structures from $n = 8$ onward. Computations predict, depending on the level of theory, 2D or 3D structures as putative energy-minimum for $n = 8$. In this work, far-infrared multiple photon dissociation spectroscopy, using Ar as tagging element, is combined with density functional theory calculations to determine the structures of Au_n^+ ($n \leq 9$) clusters formed by laser ablation. While the Au frameworks in $Au_6Ar_m^+$ and $Au_7Ar_m^+$ complexes are confirmed to be planar and that in $Au_9Ar_m^+$ three-dimensional, we demonstrate the coexistence of 3D and planar $Au_8Ar_m^+$ ($m = 1–3$) isomers. Thus, it is revealed that at finite temperatures, the formal 2D to 3D transition takes place at n=8.

I. INTRODUCTION

Small gold clusters have for decades been a subject of intensive research [1, 2, 3]. Considering that bulk gold is one of the most unreactive metals in the periodic table, the selective reactivity of gold clusters has drawn particular attention: below a certain critical size, gold clusters are reactive towards CO [4, 5] and propene [6], can co-adsorb O_2 and CO to form CO_2 [7], and can form covalent bonds with noble gases [8]. These remarkable and rather counter-intuitive reactive properties of gold clusters depend crucially on both their geometric and electronic structures [9].

To understand the interplay of geometry and electronic structure, it is essential to determine the structures and possible isomeric forms of those clusters. For instance, it is now known that neutral Au_{20} adopts a tetrahedral (pyramidal) structure [10, 11, 12], and that anionic gold clusters form hollow cages [13]. The relativistic character of gold [14] is manifested when comparing the predicted and experimentally observed structures of Au clusters with those of Cu_n and Ag_n [15, 16]. While Cu and Ag clusters adopt 3D structures from $n = 5$, Au clusters retain planar geometries up to significantly larger n.

A long-standing question, only partly answered, is the precise size at which $Au_n^{-/0/+}$ clusters become three-dimensional. For anionic Au_n^- clusters, it has been concluded that this transition takes place at $n = 12$ [17, 18, 19], whereas for neutral Au_n clusters, the 2D-3D transition was shown to occur at $n = 11$ [20]. For cationic Au_n^+ clusters, however, no conclusive answer has been achieved. Ion mobility spectrometry (IMS) experiments indicate that the transition takes place at $n = 8$ [21]. Supporting evidence for this size was found by UV/Visible (UV/Vis) photodissociation spectroscopy [22], a technique that predominantly probes the electronic structure. In addition, density functional theory (DFT) calculations show that several 2D and 3D isomers of Au_8^+ are very close in energy (differences <0.1 eV), and that their energetic ordering strongly depends on the applied levels of theory [23, 24, 25, 26]. Moreover, temperature can play an important role and multiple isomers could coexist in molecular beams, the widely used environment to probe cluster structure [27]. One can thus not rely on DFT calculations alone to determine the structures of Au_n^+ clusters. To further illustrate this issue, the IMS assignment was achieved by comparing the experiment with calculated geometric cross-sections for only two isomers, a 2D and a 3D structure, and a better agreement was found for the higher-energy isomer. IR spectroscopy has so far only been used for structure determination (by means of photofragmentation of Au_n^+-Ar complexes) for $n \leq 5$ [28, 29] and thus did not address the 2D–3D transition. Even for some of the small sizes, no consensus has been achieved about their precise geometry, e.g., the interpretation of photodissociation experiments of Au_4^+ (and its Ar complexes) to the sole existence of a rhombus Au framework [29, 30, 31, 32] was recently put in perspective by UV/Vis spectra pointing at the co-existence of a Y-shaped isomer [33].

In this work, the structures of small cationic Au_n^+ ($n \leq 9$) clusters, formed in a molecular beam, are characterized by combining far-infrared multiple-photon dissociation (IRMPD) spectroscopy and DFT calculations. Ar is used as tagging element in the experiments. The current experiments are able to go beyond previous work [28, 29] by (1) extending the frequency range probed and (2) making use of the intracavity free-electron laser FELICE [34]. The large pulse energy allows for a substantially enlarged interaction volume formed by the overlap between the molecular beam and the laser light. This enlarged interaction volume allows for the investigation of a large number of clusters per laser shot, significantly improving the signal-to-noise (s/n) ratio. The effect of Ar attachment, however, should be considered carefully, since van De Waals interactions can play a

[a] KU Leuven, Department of Physics and Astronomy, Quantum Solid-State Physics, 3001 Leuven, Belgium.
[b] Radboud University, Institute for Molecules and Materials, FELIX Laboratory, 6525 ED Nijmegen, The Netherlands.
[c] Université Grenoble Alpes, LIPhy, CNRS, 38000 Grenoble, France.

Electronic Supplementary Information (ESI) available: Calculated adsorption energies, integrated intensities in the mass spectrum, dependence of calculated infrared spectra on anharmonic effects and different positions of the Ar atoms, and Cartesian coordinates of computed structures. See DOI: 10.1039/x0xx00000x

crucial role in the energy ordering between isomers [20]. If available, the IR spectra of clusters with a different number of attached Ar atoms are discussed.

II. METHODS

The Au_n^+ clusters are produced by laser ablation at a source temperature of 200 K [35]. $Au_nAr_m^+$ complexes are obtained by adding 2% Ar in the He carrier gas. The formed cluster beam is shaped by a skimmer and a 1 mm slit aperture and the size distribution is probed by a reflectron time-of-flight mass spectrometer, right after interacting with IR light. IR spectra are obtained by comparing cluster–Ar complex intensities in mass spectra with (I) and without (I_0) IR light interaction. The IRMPD yield is calculated as $Y_{IR} = -\ln(I/I_0) / E_{IR}$, where E_{IR} is the normalized laser pulse energy. Under the applied experimental conditions, several Ar atoms are attached per Au_n^+ cluster.

The use of a tagging element in the experiments is essential, since recording an IR spectrum requires the fragmentation of the investigated clusters under IR light irradiation [36]. Fragmentation of the bare Au_n^+ clusters is difficult, even when using FELICE, due to the high dissociation energies of gold clusters. The dissociation energies, however, are much lower for the $Au_nAr_m^+$ complexes, via the Ar loss channel. In addition, investigating the bare clusters leads to contaminated spectra due to the fragmentation of larger clusters. Necessarily, the drawback of the messenger approach is that IR spectra contain structural information about the $Au_nAr_m^+$ complexes, which could be different from that of the bare Au_n^+ clusters.

Since several Ar atoms are attached per cluster under the applied experimental conditions, depletion spectra (intensity decrease upon laser interaction) must be analyzed carefully. The depletion spectrum of the $Au_nAr_m^+$ complex may be contaminated by simultaneous IR-induced fragmentation of $Au_nAr_{m+1}^+ \rightarrow Au_nAr_m^+ + Ar$, giving an intensity increase for $Au_nAr_m^+$. This process can appear in the spectrum of $Au_nAr_m^+$ as an – unphysical – negative IRMPD yield, but could also lead to a (partial) screening of a band of $Au_nAr_m^+$. Argon attachment may distort the structure of the Au_n^+ framework. To clarify the influence of Ar attachment, we analyze IR spectra of $Au_nAr_m^+$ complexes with different values of m, even though in some cases the spectra are partially contaminated from the fragmentation of complexes with more Ar atoms.

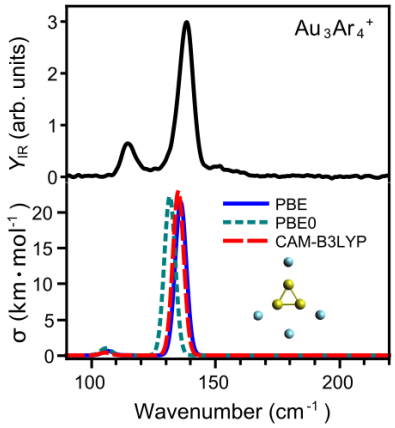

Figure 1. Experimental (top) and simulated (bottom) IR spectra of the $Au_3Ar_4^+$ complex. The simulated IR spectra are calculated using three exchange-correlation functionals (PBE, PBE0 and CAM-B3LYP). The cluster structure is shown as inset, with Au depicted in yellow, and Ar in cyan spheres.

Experiments are complemented by DFT calculations performed with the ORCA 4.1.1 software package [37], employing the dispersion-corrected (D3BJ) PBE functional in combination with the Def2-TZVPP basis set and Def2-ECP pseudopotentials. To choose this level of theory, we have used the IR spectrum of the $Au_3Ar_4^+$ complex for reference, since there is no doubt about the geometry adopted by the Au_3^+ framework. The analysis is presented in Figure 1, showing the recorded IRMPD signal in the top panel. The spectrum is similar to that measured previously [28], but with a significantly higher s/n ratio. The IRMPD spectrum of the $Au_3Ar_4^+$ complex has one intense band at 130 cm^{-1} and a weaker mode at 114 cm^{-1}. Calculations were performed using three exchange-correlation functionals: PBE, PBE0 and CAM-B3LYP, as shown in the bottom panel of the figure. Overall, the three methods show an excellent agreement with the experimental result, although PBE and CAM-B3LYP perform slightly better than PBE0. Since PBE is computationally cheaper than CAM-B3LYP, the PBE functional in conjunction with the Def2-TZVPP basis set was thus chosen. No scaling factor is used for $n \leq 5$, while a scaling factor of 1.05 is used for $n \geq 6$.

III. RESULTS AND DISCUSSION

The results for n = 4 are presented in Figure 2 with complexes $Au_4Ar_3^+$ and $Au_4Ar_4^+$ in panels (a) and (b), respectively. The IRMPD spectrum of $Au_4Ar_3^+$ has two bands, at 91 cm^{-1} (or lower, since this is the lowest wavenumber of the probed spectral range) and 107 cm^{-1}, whereas that for $Au_4Ar_4^+$ shows bands centered at 103 and 158 cm^{-1}. Fragmentation of $Au_4Ar_4^+$ is evidenced in the spectrum for $Au_4Ar_3^+$ at 158 cm^{-1}, by a negative IRMPD signal; it appears likely that the intensity with which the 107 cm^{-1} band is observed for $Au_4Ar_3^+$ is also affected by fragmentation from the $Au_4Ar_4^+$ band centered at 103 cm^{-1}. The bands observed for $Au_4Ar_4^+$ agree well with previous measurements [29], and each experimental spectrum shows an excellent agreement with calculated (unscaled) harmonic vibrational spectra of the rhombic Au_4^+ framework, shown below the experimental spectra. Spectra of $Au_4Ar_m^+$ complexes with $m \leq 2$ only show ingrowth and are thus not useful for further analysis.

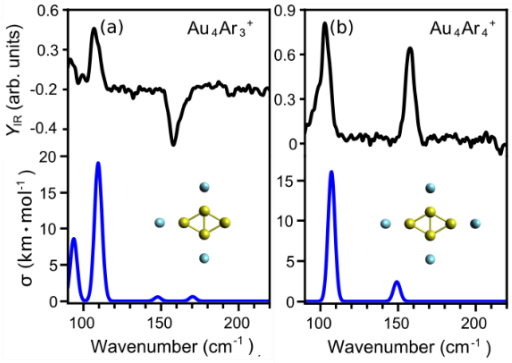

Figure 2. Experimental (top, black) and simulated (bottom, blue) IR spectra of (a) $Au_4Ar_3^+$, and (b) $Au_4Ar_4^+$. The spectrum of $Au_4Ar_3^+$ shows partial signal ingrowth caused by fragmentation of $Au_4Ar_4^+$.

For n = 5, spectra could be recorded for three Ar complexes, shown in Figure 3: (a) $Au_5Ar_3^+$, (b) $Au_5Ar_4^+$ and (c) $Au_5Ar_5^+$. Partial signal ingrowth is present for the spectra of $Au_5Ar_3^+$ and $Au_5Ar_4^+$, strongly affecting bands observed around 110 cm^{-1}. For $Au_5Ar_3^+$, an additional band is found at 184 cm^{-1}. The spectrum of the $Au_5Ar_5^+$ complex shows five clear bands, two of which were either out of range (102 cm^{-1}) or unresolved (212 cm^{-1}) in previous experiments

[29]. Complexes with $m \leq 2$ only show signal ingrowth. Despite the affected spectra for $Au_5Ar_3^+$ and $Au_5Ar_4^+$, the agreement between the experiment and the calculations is excellent for the three Ar complexes, demonstrating that the Au_5^+ framework adopts a planar bow-tie structure. We do note, however, small frequency mismatches. For a perfect match, a scaling factor of 1.04 would be required, which is not applied in the figure. The need for such a scaling in IR spectra of gold clusters calculated by DFT is well known [38]. Nevertheless, the overall correspondence for m = 3, 4, and 5 is excellent, making the structural assignments of the gold frameworks in $Au_nAr_m^+$ (n = 3-5) unambiguous.

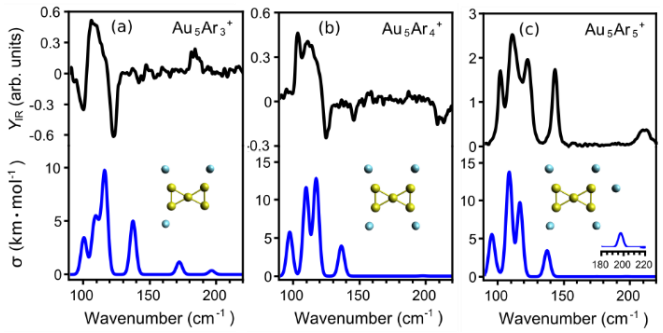

Figure 3. Experimental (top, black) and simulated (bottom, blue) IR spectra of (a) $Au_5Ar_3^+$, (b) $Au_5Ar_4^+$, and (c) $Au_5Ar_5^+$. The spectra of $Au_5Ar_3^+$ and $Au_5Ar_4^+$ show partial signal ingrowth due to fragmentation of $Au_5Ar_4^+$ and $Au_5Ar_5^+$.

For $n \geq 6$, the s/n ratios of the observed IRMPD spectra are a bit lower because intensities of those complexes are smaller (integrated intensities of a representative mass spectrum are shown in the ESI). Nevertheless, the spectra are of sufficient quality for structural assignment. In the IRMPD spectrum of $Au_6Ar_2^+$ (Figure 4a), four bands are observed at 97, 128, 158, and 195 cm^{-1}. Two planar Au_6^+ isomers are considered in the discussion; the lowest-energy structure (Iso1) is constructed by adding a Au atom to the Au_5^+ bow-tie isomer, while the second isomer (Iso2) has a triangular shape. In our calculations, Iso2 is 0.15 eV higher in energy (relative energies for bare Au_6^+). Distinction between both isomers was not possible in IMS experiments, due to their similar collisional cross sections [21]. As shown in Figure 4a, Iso1 correctly reproduces the four bands of the IRMPD spectrum for $Au_6Ar_2^+$, apart from a computed double peak around 100 cm^{-1}. Those modes may be too close to be distinguished experimentally, or the intensity of the second mode may be overestimated in the calculation. Iso2 can be disqualified as responsible for the IRMPD spectrum since its simulated IR spectrum misses the band at 158 cm^{-1} and has a mode at 175 cm^{-1} that is absent experimentally. The analysis for the spectrum of $Au_6Ar_3^+$, shown in panel (b), is similar. In this case, a single intense band is seen at 95 cm^{-1}, possibly together with a weaker mode around 159 cm^{-1}. The calculations for $Au_6Ar_3^+$ also seem to indicate that Iso1 is the complex present in the cluster beam, matching better the positon of the band at 95 cm^{-1} and predicting a second mode at 156 cm^{-1}, thus close to the potential second band. The IRMPD spectrum of the complex with a single attached Ar atom only shows ingrowth. Nevertheless, the noise level in these spectra is relatively high; combining the calculated IR bands of both isomers shows that a population up to a 20% of Iso2 in $Au_6Ar_3^+$ would still be consistent with the data. For $Au_6Ar_2^+$, in contrast, even a 5% contribution of Iso2 would be inconsistent with the measurement.

For n = 7, the spectra of two Ar complexes are considered, as shown in Figure 5: (a) $Au_7Ar_2^+$; and (b) $Au_7Ar_3^+$. In both cases, the experiment yields three clear bands at 91, 136, and 192 cm^{-1}. Based on IMS measurements, Au_7^+ was predicted to have a centered hexagonal structure [21]. This planar structure (with a slight out-of-plane distortion) was also the lowest-energy isomer in previous DFT studies [24, 25, 26]. The calculated vibrational spectra of both Ar complexes, with the hexagonal Au_7^+ framework, are in very good agreement with the IRMPD spectra.

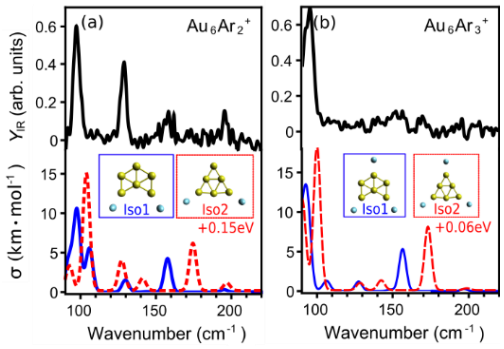

Figure 4. Experimental (top, black) and simulated (bottom, blue and red) IR spectra of (a) $Au_6Ar_2^+$, and (b) $Au_6Ar_3^+$.

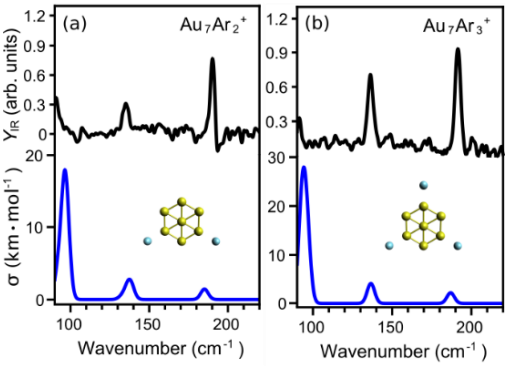

Figure 5. Experimental (top, black) and simulated (bottom, blue) IR spectra of (a) $Au_7Ar_2^+$, and (b) $Au_7Ar_3^+$.

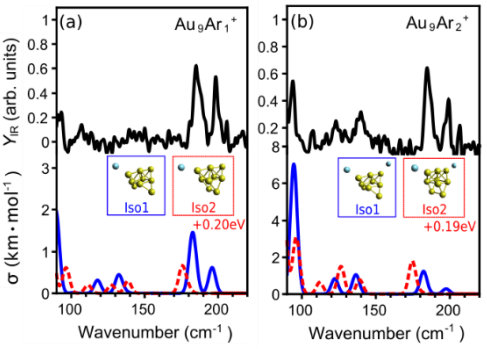

Figure 6. Experimental (top, black) and simulated (bottom, blue and red) IR spectra of (a) $Au_9Ar_1^+$, and (b) $Au_9Ar_2^+$.

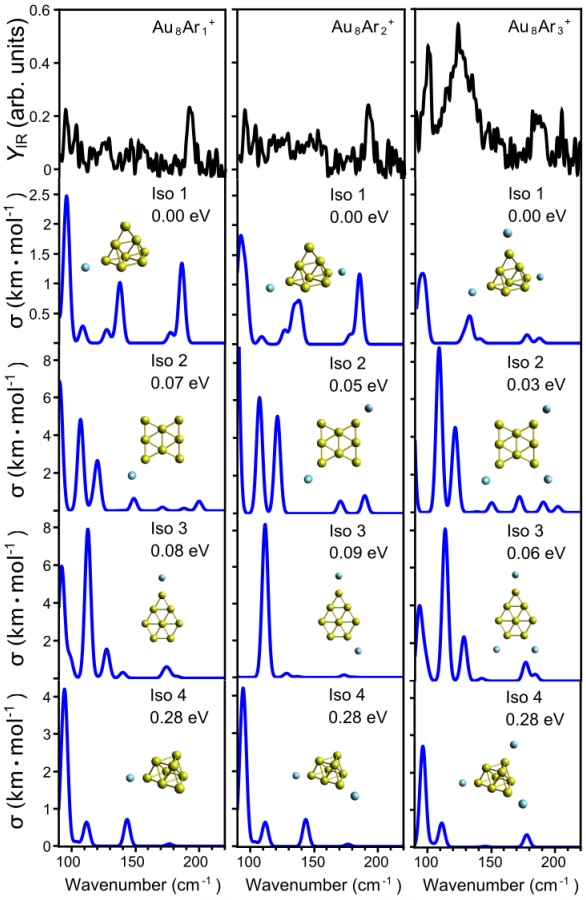

Figure 7. Experimental (top, black) and simulated (bottom, blue) IR spectra of $Au_8Ar_1^+$ (left), $Au_8Ar_2^+$ (middle) and $Au_8Ar_3^+$ (right). Four different low-lying isomers are considered.

For the largest cluster size considered in this study, n = 9, the complexes (a) $Au_9Ar_1^+$, and (b) $Au_9Ar_2^+$ (Figure 6) are discussed. In both cases, two pronounced bands are found at 185 and 199 cm^{-1}, in addition to three modes for $Au_9Ar_2^+$ at 94, 123 and 140 cm^{-1}. For $Au_9Ar_1^+$, these modes may be present in the experimental data, but hidden in the noise level. The calculations considered two three-dimensional isomers for the Au_9^+ framework, as suggested in Ref. [27]. For both Ar complexes, the IRMPD spectrum agrees very well with the calculated IR spectra of the lowest-energy complexes, in particular predicting the two intense modes above 180 cm^{-1}, which are absent for Iso2.

Thus, whereas the Au framework in Au_7^+ is still planar, in Au_9^+ it adopts a 3D configuration. The precise 2D–3D transition size therefore depends on the inferred structure for Au_8^+. In Figure 7, the IRMPD spectra of $Au_8Ar_1^+$, $Au_8Ar_2^+$, and $Au_8Ar_3^+$ are presented. The spectra of $Au_8Ar_1^+$ and $Au_8Ar_2^+$ have a rather low s/n, with only one clear mode at 192 cm^{-1} in both cases. The IRMPD spectrum of $Au_8Ar_3^+$, in contrast, shows a band close to 100 cm^{-1}, a broad feature around 125 cm^{-1}, and a third band at 185 cm^{-1}. Four isomers were considered in the computations: Iso1 (3D), the structure proposed by IMS [21], is formed by removing a low-coordinated atom of Au_9^+. Iso2 and Iso3 are planar, and Iso4 is a doubly capped bipyramid, another 3D isomer. Previous DFT studies using a plane-wave approach found Iso2 as the lowest in energy when employing the PBE and TPSS functionals, while Iso4 was found by applying M06-L [23]. Iso3 was also considered in these theoretical studies. In our calculations for the bare Au_8^+ cluster, the energy ordering is Iso1 (0.00 eV) < Iso3 (0.08 eV) < Iso2 (0.09 eV) < Iso4 (0.27 eV). Isomers 1 to 3 are thus very close in energy. Upon Ar attachment, the relative energies vary slightly; the values are given in Figure 7.

Both 3D isomers (Iso1 and Iso4) have their main vibrational modes between 60 and 80 cm^{-1}, below the experimental lower limit of 90 cm^{-1}, and only weak modes in the recorded spectral range (note the different y-axis ranges in Figure 7). Nevertheless, the mode at 192 cm^{-1} in the spectra of $Au_8Ar_1^+$ and $Au_8Ar_2^+$ agrees well with the simulations for Iso1. The low s/n ratio of the spectra below 180 cm^{-1}, however, does not allow to eliminate contributions from Iso2 and Iso3 to the IRMPD spectra. For $Au_8Ar_3^+$, the three bands observed in the IRMPD spectrum are consistent with the calculated spectrum for Iso1; only the middle band is a bit blue-shifted with respect to the experiment (137 cm^{-1} versus 125 cm^{-1}). This mismatch could be explained by invoking the isomeric presence of one or both planar isomers (Iso2 and Iso3). The strongest bands for these isomers are predicted such that depletion signals stemming from Iso2 and/or Iso3 could merge with those from Iso1, forming the band centered at 125 cm^{-1}, thereby explaining its relative width. Since Iso2 and Iso3 present several modes of relatively high intensity between 100 and 130 cm^{-1}, any signal recorded experimentally is biased towards planar structures. Thus, the spectra show that the isomeric population is dominated by the 3D Iso1. Nevertheless, this analysis shows that Ar complexes formed by planar isomers of the Au_8^+ framework are likely present in the cluster beam, especially for the $Au_8Ar_3^+$ complex. The possibility that complexes with the same metal framework but other positions of the Ar atoms are present, cannot be excluded (see supporting information). While Ar attachment at different configurations does not have a major effect in the positions of the IR bands, it does modify their relative intensity. In addition, the effect of including anharmonicities in the calculations is presented in the supporting information, showing that anharmonic effects have only a minor influence in the IR spectra.

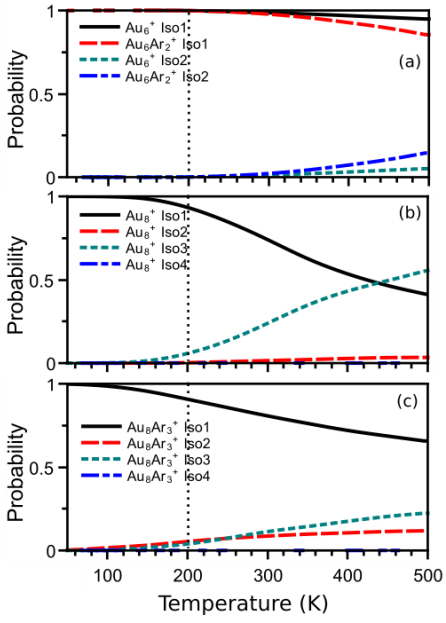

Figure 8. Relative probability versus temperature of finding different isomers in the cluster beam assuming full thermalization. (a) Isomers 1 and 2 of Au_6^+ and $Au_6Ar_2^+$. (b) Isomers 1 to 4 of Au_8^+. (c) Isomers 1 to 4 of $Au_8Ar_3^+$.

Since the computed energy differences between the Au_8^+ isomers (iso1, iso2, iso3, and iso4) are very small, different isomers may coexist in the molecular beam. To investigate this on more quantitative grounds, one needs to consider the finite temperature at which experiments are performed (200 K). The structures obtained by DFT can be used to calculate the thermal population of each isomer *i* as a function of temperature, from the knowledge of relative energies E_i, vibrational frequencies ω_i^α (α ranging from 1 to 3*n*-6) and point group with order m_i. The (quantum) partition function associated with isomer i is calculated as:

$$Z_i = \frac{2}{n!\, m_i} \exp(-\beta E_i) \prod_\alpha \frac{\exp(-\beta\hbar\omega_i^\alpha/2)}{1-\exp\left(-\beta\hbar\omega_i^\alpha\right)}, \qquad (1)$$

with $\beta_i = (k_B T)^{-1}$. Then, the probability of finding isomer i at temperature T is

$$p_i = {Z_i}\Big/{\sum_j Z_j}. \qquad (2)$$

The analysis was performed for Au_6^+ and Au_8^+. The results are summarized in Figure 8. In panel (a) the temperature-dependent populations of the two isomers of Au_6^+ and $Au_6Ar_2^+$ are presented. For this cluster size, both the bare and Ar-tagged Iso2 isomers do not compete with the lowest-energy structures. For Au_8^+ and $Au_8Ar_3^+$, in contrast, due to the close relative energies between the different isomers, the statistical analysis predicts coexistence between the 3D Iso1 and both planar isomers (Iso2 and Iso3) at 200 K. The 3D Iso4 is too high in energy to compete. The relative populations, however, will depend strongly on the precise energy difference between isomers.

IV. CONCLUSIONS

In conclusion, IRMPD spectroscopy was combined with DFT calculations to determine the geometries of $Au_nAr_m^+$ clusters in the $n \leq 9$ size range, taking advantage of the FELICE intracavity free-electron laser enabling high s/n ratio IR spectra. The structure of Au_6^+ has been assigned for the first time; this structure is formed by adding a Au atom to the bow-tie Au_5^+ cluster. The structure of Au_7^+ is found to be a planar hexagon with a central Au atom, showing that all clusters with $n \leq 7$ adopt planar structures, whereas for Au_9^+ a three-dimensional structure is confirmed. The critical cluster size for determining the 2D to 3D transition of the gold cluster cations is therefore $n = 8$. At this size, good agreement is found with a 3D structure, but evidence is found for the coexistence of one or a combination of two planar isomers. In our calculations, the three isomers are found to be almost isoenergetic, within the typical uncertainty of conventional DFT. Our experimental evidence for co-existence thus confirms the reliability of current quantum chemical methods.

Conflicts of interest

There are no conflicts to declare.

Acknowledgment

This work has been supported by the KU Leuven Research Council (project C14/18/073) and by the European Community's Horizon 2020 Framework Programme under grant agreement nº 654148. P.F. acknowledges the Research Foundation – Flanders (FWO) for a postdoctoral grant. We gratefully acknowledge the Nederlandse Organisatie voor Wetenschappelijk Onderzoek (NWO) for the support of the FELIX Laboratory and thank the FELIX staff. P.F. thanks Laia Delgado Callicó for useful theoretical discussions.

References

1. H. Häkkinen, *Adv. Phys. X* **2016**, *1*, 467.
2. M. Haruta, N. Yamada, T. Kobayashi, S Iijima, *J. Catal.* **1989**, *115*, 301.
3. K. Hansen, P. Ferrari, E. Janssens, P. Lievens, *Phys. Rev. A* **2017**, *96*, 022511.
4. M. Neumaier, F. Weigend, O. Hampe, M. M. Kappes, *J. Chem. Phys.* **2005**, *122*, 104702.
5. N. Veldeman, P. Lievens, M. Andersson, *J. Phys. Chem. A* **2005**, *109*, 11793–11801.
6. E. Janssens, H. T. Le, P. Lievens, *Chem. Eur. J.* **2015**, *21*, 15256–15262.
7. W. T. Wallace, R. L. Whetten, *J. Am. Chem. Soc.* **2002**, *124*, 7499.
8. S. Pan, G. Jana, B. Merino, P. K. Chattaraj, *ChemistryOpen* **2019**, *8*, 173.
9. P. Ferrari, J. Vanbuel, E. Janssens, P. Lievens, *Acc. Chem. Res.* **2018**, *51*, 3174.
10. P. Gruene, D. M. Rayner, B. Redlich, A. F. G. van der Meer, J. T. Lyon, G. Meijer, A. Fielicke, *Science* **2008**, *321*, 674.
11. J. Li, X. Li, H.-J. Zhai, *Science* **2003**, *299*, 864.
12. Z. Li, H.-Y. Tiffany Chen, K. Schouteden, T. Picot, T.-W. Liao, A. Seliverstov, C. Van Haesendonck, G. Pacchioni, E. Janssens, P. Lievens, *Sci. Adv.* **2020**, *6*, 1.
13. S. Bulusu, X. Li, L. Wang, X. C. Zeng, *Proc. Natl. Acad. Sci.* **2006**, *103*, 8326.
14. P. Pyykko, *Chem. Rev.* **1988**, *88*, 563-594.
15. O. V. Lushchikova, D. M. M. Huitema, P. López-Tarifa, L. Visscher, Z. Jamshidi, J. M. Bakker, *J. Phys. Chem. Lett.* **2019**, *10*, 2151.
16. J. van der Tol, D. Jia, Y. Li, V. Chernyy, J. M. Bakker, M. T. Nguyen, P. Lievens, E. Janssens, *Phys. Chem. Chem. Phys.* **2017**, *19*, 19360.
17. F. Furche, R. Ahlrichs, P. Weis, C. Jacob, S. Gilb, T. Bierweiler, M. M. Kappes, *J. Chem. Phys.* **2002**, *117*, 6982.
18. H. Häkkinen, B. Yoon, U. Landman, X. Li, H.-J. Zhai, L.-S. Wang, *J. Phys. Chem. A* **2003**, *107*, 6168.
19. X. Xing, B. Yoon, U. Landman, J. H. Parks, *Phys. Rev. B* **2006**, *74*, 165423.
20. B. R. Goldsmith, J. Florian, J.-X. Liu, P. Gruene, J. T. Lyon, D. M. Rayner, A. Fielicke, M. Scheffler, L. M. Ghiringhelli, *Phys. Rev. Materials* **2019**, *3*, 016002.
21. S. Gilb, P. Weis, F. Furche, R. Ahlrichs, M. M. Kappes, *J. Chem. Phys.* **2002**, *116*, 4094.
22. A. N. Gloess, H. Schneider, J. M. Weber, M. M. Kappes, *J. Chem. Phys.* **2008**, *128*, 114312.
23. L. Ferrighi, B. Hammer, G. K. H. Madsen, *J. Am. Chem. Soc.* **2009**, *131*, 10605.
24. P. Ferrari, H. A. Hussein, C. J. Heard, J. Vanbuel, P. Lievens, R. L. Johnston, E. Janssens, *Phys. Rev. A* **2018**, *97*, 052508.
25. F. Remacle, E. S. Kryachko, *J. Chem. Phys.* **2005**, *122*, 044304.
26. E. M. Fernández, J. M. Soler, I. L. Garzón, L. C. Balbás, *Phys. Rev. B* **2004**, *70*, 165403.
27. P. Weis, T. Bierweiler, E. Vollmer, M. M. Kappes, *J. Chem. Phys.* **2002**, *117*, 9293.
28. A. Shayeghi, R. L. Johnston, D. M. Rayner, R. Schfer, A. Fielicke, *Angew. Chem. Int. Ed.* **2015**, *54*, 10675.
29. A. Shayeghi, R. Schäfer, D. M. Rayner, R. L. Johnston, A. Fielicke, *J. Chem. Phys.* **2015**, *143*, 024310.
30. A. Schweizer, J. M. Weber, S. Gilb, H. Schneider, D. Schooss, M. M. Kappes, *J. Chem. Phys.* **2003**, *119*, 3699.
31. V. Kaydashev, P. Ferrari, C. Heard, E. Janssens, R. L. Johnston, P. Lievens, *Part. Part. Syst. Charact.* **2016**, *33*, 364–372.
32. A. Shayeghi, R. L. Johnston, R. Schäfer, *Phys. Chem. Chem. Phys.* **2013**, *15*, 19715-19723.
33. M. Forstel, W. Schewe, O. Dopfer, *Angew. Chem. Int. Ed.*, **2019**, *58*, 3356.
34. J. M. Bakker, V. J. F. Lapoutre, B. Redlich, J. Oomens, B. G. Sartakov, A. Fielicke, G. von Helden, G. Meijer, A. F. G. van der Meer, *J. Chem. Phys.* **2010**, *132*, 074305.

35. P. Ferrari, J. Vanbuel, T.-W. Liao, Y. Li, E. Janssens, P. Lievens, Modifications of gas aggregation sources: The Double Laser Ablation Source Approach, in Gas Aggregation Synthesis of Nanoparticles, Ed. I. Huttel, Weinheim, Wiley-VCH, *2017*, pp. 57-78.
36. A. Fielicke, A. Kirilyuk, C. Ratsch, J. Behler, M. Scheffler, G. von Helden, G. Meijer, *Phys. Rev. Lett.* **2004**, *93*, 023401.
37. F. Neese, *Rev.: Comput. Mol. Sci.* **2012**, *2*, 73.
38. L. A. Mancera, D. M. Benoit, *Phys. Chem. Chem. Phys.* **2013**, *15,* 192.